Biophysical Chemistry 253 (2019) 106213

Contents lists available at ScienceDirect

Biophysical Chemistry

journal homepage: www.elsevier.com/locate/biophyschem

Research Article

Structure-based derivation and intramolecular cyclization of peptide inhibitors from PD-1/PD-L1 complex interface as immune checkpoint blockade for breast cancer immunotherapy

Kun Zhou[a], Ji Lu[b], Xiaoxin Yin[b], Han Xu[b], Longzhi Li[b], Baojin Ma[a,*]

[a] Department of General Surgery, Huashan Hospital Affiliated to Fudan University, Shanghai 200040, China
[b] Department of General Surgery, Jing'an District Center Hospital of Shanghai, Huashan Hospital Fudan University Jing'an Branch, Shanghai 200040, China

HIGHLIGHTS

- Linear self-inhibitory peptides are stripped from the active finger of PD-1/PD-L1 complex.
- The linear peptides exhibit large flexibility and would be unfavorable to rebind at the complex interface.
- Cyclization strategy is used to improve peptide affinity by reducing the flexibility.
- Designed cyclic peptides are found to have increased affinity relative to linear peptides.

GRAPHICAL ABSTRACT

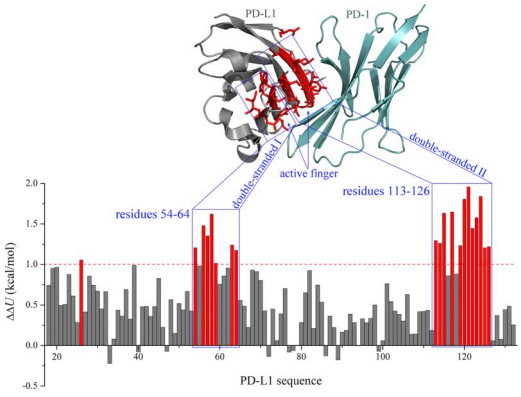

ARTICLE INFO

Keywords:
Immune checkpoint
PD-1/PD-L1
Breast cancer immunotherapy
Self-inhibitory peptide
Cyclic peptide
Intramolecular cyclization

ABSTRACT

The interaction event between programmed death receptor-1 (PD-1) and its ligand (PD-L1) functions as an essential immune checkpoint against cytotoxic T effector cell activation. Previously, a number of small-molecule inhibitors and antibody drugs have been successfully developed to block the PD1/PDL1 signaling axis for breast cancer immunotherapy. Here, we attempt to directly disrupt the formation of PD-1/PD-L1 complex by using a self-inhibitory peptide (SIP) strategy. In the procedure, the complex crystal structure is examined systematically with energetic analysis and alanine scanning. Two double-stranded segments I and II in PD-L1 active finger are identified as hotspot regions; they directly interact with the amphipathic pocket of PD-1 to form the complex system. The segments are derived from PD-L1 to define two SIP peptides, namely, DS-I and DS-II, which are thought to have capability of rebinding at the complex interface, thus disrupting PD-1/PD-L1 interaction as a new immune checkpoint blockade. A further analysis reveals that the free linear DS-I and DS-II peptides are highly flexible without protein context support, which would incur a large entropy penalty (unfavorable indirect readout effect) when rebinding to PD-1. Next, intramolecular cyclization is applied to constraining the intrinsically disordered conformation of free DS-II peptide into native ordered double-stranded configuration, which can be substantiated by molecular dynamics simulation and circular dichroism spectroscopy. Several cyclized counterparts of linear DS-II peptide are designed and their affinities to PD-1 are determined using fluorescence polarization assays. As might be expected, three designed cyclic peptides DS-II[c111–127], ΔDS-II

* Corresponding author.
E-mail address: baojinma@sina.cn (B. Ma).

https://doi.org/10.1016/j.bpc.2019.106213
Received 3 May 2019; Received in revised form 24 June 2019; Accepted 25 June 2019
Available online 26 June 2019

[c111–127] and ΔDS-II[c110–128] exhibit considerably increased potency (K_d = 28.0 ± 4.2, 17.5 ± 3.1 and 11.6 ± 2.3 μM, respectively) relative to linear DS-II peptide (K_d = 109 ± 15 μM).

1. Introduction

Tumor immune microenvironment encompasses a wide range of complex interactions between tumor cell, immune cells, and tumor stroma, which are regulated by a series of immune checkpoint (IC) events. ICs are a kind of signals for regulating antigen recognition in the process of immune response; they consist of both co-stimulatory (such as CD28, ICOS, and CD137) and co-inhibitory (such as PD-1, CTLA-4, and VISTA) pathways that are important for maintaining self-tolerance and regulating the type, magnitude, and duration of the immune response [1]. Since immune checkpoints are initiated by the receptor/ligand interactions that can be readily blocked by antibodies and chemical agents or modulated by recombinant forms of ligands or receptors, they have been recognized as a new and promising druggable target of diverse cancers [2].

In breast cancer, immune checkpoint mechanism is often activated to suppress the nascent anti-tumor immune response. This has led to the development of several cancer checkpoint inhibitors or antibody drugs that are currently being tested in clinical trials or have been approved for anti-breast cancer therapy [3]. Blocking the activities of these checkpoint proteins with monoclonal antibodies, small molecules and macrocyclic inhibitors, and thus restoring T cell function, has delivered breakthrough therapies against cancer [3–5]. Programmed death receptor-1 (PD-1) is an inhibitory transmembrane protein expressed on T cells, B cells, and NK cells. The interaction between PD-1 and its ligand (PD-L1) functions as an immune checkpoint against unrestrained cytotoxic T effector cell activity; it promotes peripheral T effector cell exhaustion and conversion of T effector cells to immunosuppressive T regulatory cells. Immune checkpoint inhibitors, which block the PD-1/PD-L1 axis and reactivate cytotoxic T effector cell function, are actively being investigated for the treatment of breast cancer [6]. For example, since the 2011 FDA approval of Ipilimumab (targeting CTLA4) for the treatment of metastatic melanoma, five additional checkpoint blockade therapies, all targeting PD-1/PD-L1 axis, have been approved for the treatment of a broad range of tumor types, including Nivolumab (targeting PD-1), Pembrolizumab (targeting PD-1), Atezolizumab (targeting PD-L1), Avelumab (targeting PD-L1) and Durvalumab (targeting PD-L1) [7]. Additionally, Ipilimumab plus Nivolumab combination therapy has been approved for the treatment of advanced melanoma with favorable outcomes compared with either monotherapy [8]. However, all these approved agents are monoclonal antibodies and there are no small-molecule inhibitors or peptide drugs available in market for checkpoint blockade therapies.

Recently, the high-resolution crystal structure of PD-1 in complex with PD-L1 has been solved by Zak et al. using X-ray crystallography (PDB: 4ZQK) [9]. As shown in Fig. 1, the active finger of PD-L1 is a four-stranded β-sheet, which consists of two sequence-disconnected, spatially vicinal double-stranded segments I and II (residues 54–68 and 110–132, respectively); they are inserted into and interact with the amphipathic pocket of PD-1 to form the complex system. Previously, based on crystal structure data we have successfully investigated the molecular mechanism of mutation-induced acquired resistance to tyrosine kinase inhibitors in ErbB2-positive breast cancer [10]. In this study, we systematically examined the binding mode and interaction details between PD-1 and PD-L1 in the complex crystal structure, from which the interfacial hotspot regions were determined. Based on the harvested knowledge, the double-stranded segments were split from the complex system and then truncated and cyclized to derive self-inhibitory peptides (SIPs) [11–14], which were designed to have capability of rebinding at the complex interface, thus disrupting PD-1/PD-L1 recognition and interaction as a new immune checkpoint blockade strategy. We also demonstrated that the cyclized PD-L1 peptides can well held in their native double-stranded configuration and can effectively bind to PD-1 by using molecular dynamics simulation, circular dichroism spectroscopy and fluorescence polarization assay.

2. Materials and methods

2.1. Computational part

The crystal structure of PD-1/PD-L1 complex was retrieved from the PDB database [15] with accession ID 4ZQK. The structure was pre-prepared by adding hydrogen atoms, assigning protonation states and mending side chains. Investigated double-stranded peptides as well as peptide/PD-1 interaction complexes were directly split from the crystal structure and treated with AMBER ff12SB force field [16]. Each system was solvated in a rectangular TIP3P water box [17]. Periodic boundary conditions were applied during the simulation in all dimensions. The distance between the wall of the box and the closest atom of the solute was 10 Å. The systems were minimized by 1000 steps of steepest descent method and 4000 steps of conjugate gradient method [18,19]. Subsequently, the systems were heated during 50 ps from 0 to 300 K, followed by 100-ns (for complexes) or 250-ns (for free peptides) simulations for equilibration and an additional production simulation for data collection [20,21]. The hydrogen atoms were constrained by performing the SHAKE method [22] and the time step was set at 2 fs. No extra restraints were set neither for the protein nor the ligand. The particle-mesh Ewald (PME) procedure [23] was used to estimate the long-range electrostatic interactions and a nonbonded cut-off distance of 10 Å was used.

Totally 1000 conformational snapshots of each simulated protein/protein or protein/peptide interaction complex were saved evenly from the last production simulation trajectory. Molecular mechanics/Poisson-Boltzmann surface area (MM/PBSA) method [24] was performed over these snapshots to analyze the total interaction energy (ΔU) of complex, which can be decomposed into nonbonded potential

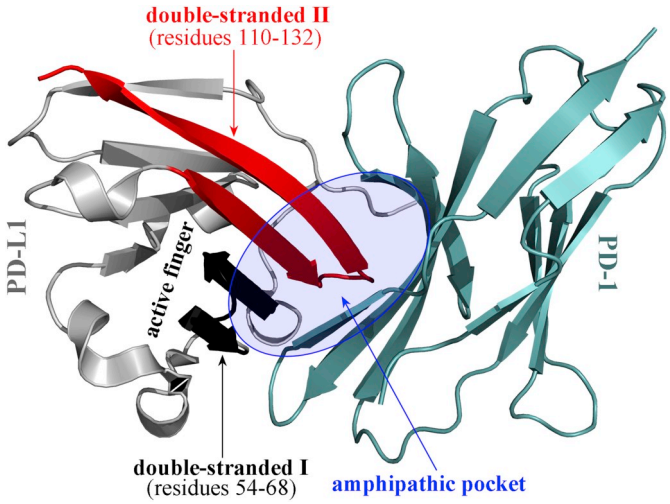

Fig. 1. Stereoview of the crystal structure of PD-1/PD-L1 complex (PDB: 4ZQK). The active finger of PD-L1 is a four-stranded β-sheet, which consists of two sequence-disconnected, spatially vicinal double-stranded segments I and II; they are inserted into and interact with the amphipathic pocket of PD-1 to form the complex system.

ΔE and desolvation effect ΔD, and calculated with molecular mechanics (MM) approach and finite-difference solution of implicit solvent model (PBSA), respectively. The conformational flexibility of helical peptides was dissected using normal mode analysis (NMA) to estimate entropy penalty $-T\Delta S$ upon the complex binding [25]. Consequently, the total binding free energy ΔG can be expressed as [26]:

$$\Delta U \leq \Delta E(i) + < \Delta D(i) >^{1000\ \text{snapshots}} \quad (1)$$

$$\Delta G = \Delta U - < T\Delta S(i) >^{100\ \text{snapshots}} \quad (2)$$

where $< \cdots >$ represents averages over multiple snapshots from a single simulation trajectory and i corresponds to the ith snapshot of the complex.

2.2. Experimental part

The binding affinity of two linear peptides DS-I and DS-II as well as three cyclic peptides DS-II[c111–127], ΔDS-II[c111–127] and ΔDS-II [c110–128] to the recombinant protein of human PD-1 were tested in this study; they are listed in Table 1. All these peptides were synthesized by Gill Biochem using Fmoc solid phase chemistry and disulfide bond oxidization in 0.1 M ammonium bicarbonate [27].

Circular dichroism (CD) analysis of linear DS-II peptide and its cyclized counterpart DS-II[c111–127] were performed on a J-810 spectropolarimeter in wavelength range from 190 to 250 nm at 25 °C using a quartz cell with of 0.1-cm path length. All CD signals were recorded at a peptide concentration 25 μM in 10 mM phosphate buffer [28]. The final spectra were expressed as mean residue ellipticity [θ] in deg. cm^2 $dmol^{-1}$, the molar ellipticity per residue.

The binding affinity of above five peptides to PD-1 was measured using a fluorescence polarization (FP) protocol as described previously [29,30]. The PD-1 protein was titrated to rhodamine-labeled peptides in a buffer (60 mM HEPES, pH 7.3, 100 mM NaCl and 5 mM DTT). For cyclic peptides the DTT was not used to avoid disulfide bond reduction [31]. A LS-55 fluorimeter was utilized to monitor FP change upon the titration, which was plotted as a function of increased titrated peptide concentration. The dissociation constants (K_d) were derived by curve fitting:

$$F = [F_0 + F_{stt}([\text{peptide}]/K_d)]/[1 + ([\text{peptide}]/K_d)] \quad (3)$$

where [peptide] is the concentration of titrated peptides, F is the measured polarization at the concentration, F_0 is the blank polarization without titration, and F_{stt} is the measured polarization at maximal titration. All experiments were performed at 25 °C and each assay was carried out in triplicate.

3. Results and discussion

3.1. Hotspot analysis of PD-1/PD-L1 complex interface

The crystal structure of human PD-1 in complex with its cognate ligand PD-L1 was subjected to 100-ns MD simulations. The dynamics trajectory indicated that the complex reaches stable state after ~30-ns simulations. Here, we ran computational alanine scanning (CAS) [32] to determine the residue importance of PD-L1 binding to PD-1 based on analysis of the last 50-ns MD equilibrium trajectory (*i.e.* 50–100 ns). In the crystal complex structure, the PD-L1 protein has residues 18–132; the scanning strategy separately mutated each residue to neutral alanine and then calculated change in total interaction energy ($\Delta\Delta U$) upon the mutation. The obtained $\Delta\Delta U$ value can be used to measure the relative contribution of each PD-L1 residue to the complex interaction potency [33–35]; the favorable and unfavorable residues in the interaction can be indicated by $\Delta\Delta U > 0$ and < 0, respectively.

As shown in Fig. 2, most PD-L1 residues are favorable for the interaction ($\Delta\Delta U > 0$). This is expected if considering that the sequence and structure of naturally evolved PD-L1 protein have already been optimized to well match its cognate receptor PD-1 and hence residue mutation would impair the matching compatibility and then cause unfavorable effect on the native receptor/ligand interaction. However, most mutations can only affect the interaction modestly or moderately, with $\Delta\Delta U < 1$ kcal/mol. This can be explained by the fact that the PD-L1 has only a small contact region (active finger) on its surface so that a majority of its residues cannot influence the interaction directly and considerably. The relatively important PD-L1 residues ($\Delta\Delta U > 1$ kcal/mol) are highlighted in Fig. 2. These residues are mostly located in the active finger region of PD-L1 and directly interact with the amphipathic pocket of PD-1; they are regarded as hotspot residues and serve as determinants of complex affinity and specificity. According to CAS characterization, the hotspot residues can be roughly divided into two sequence-disconnected regions, separately covering residues 54–64 and 113–126, which are basically overlapped with the double-stranded I and II, respectively, indicating that the two double strands play a crucial role in PD-1/PD-L1 recognition and interaction. We herein considered that the double-stranded segments can be used as SIP peptides to target the complex interaction [11].

3.2. Conformational stability and binding capability of double-stranded peptides

According to above analysis, the PD-1/PD-L1 complex system can be regarded as a peptide-medicated protein–protein interaction, where the complex is formed by binding of two hotspot regions (*i.e.* double-stranded segments I and II) in PD-L1 active finger to the amphipathic pocket of PD-1. The segments I and II were split from the PD-L1 active finger to derive DS-I peptide (^{54}IVYWEMEDKNIIQFV^{68}) and DS-II

Table 1
The calculated binding energetics and measured binding affinity of PD-L1 derived linear peptides DS-I and DS-II as well as cyclic peptides DS-II[c111–127], ΔDS-II [c111–127] and ΔDS-II[c110–128] to PD-1.

Peptide	Sequence	Energetics (kcal/mol)			Affinity K_d (μM)
		ΔU	$-T\Delta S$	ΔG	
DS-I	^{54}IVYWEMEDKNIIQFV^{68}	−37.4	34.6	−2.8	n.d.[a]
DS-II	^{110}GVYRCMISYGGADYKRITVKVNA^{132}	−69.2	54.3	−14.9	109 ± 15
DS-II[c111–127]	^{110}GCYRCMISYGGADYKRICVKVNA^{132}	−66.2	38.7	−27.5	28.0 ± 4.2
ΔDS-II[c111–127]	^{111}CYRCMISYGGADYKRIC^{127}	−61.8	30.5	−31.3	17.5 ± 3.1
ΔDS-II[c110–128]	^{110}CVYRCMISYGGADYKRITC^{128}	−63.0	32.9	−30.1	11.6 ± 2.3

[a] n.d., not detectable.

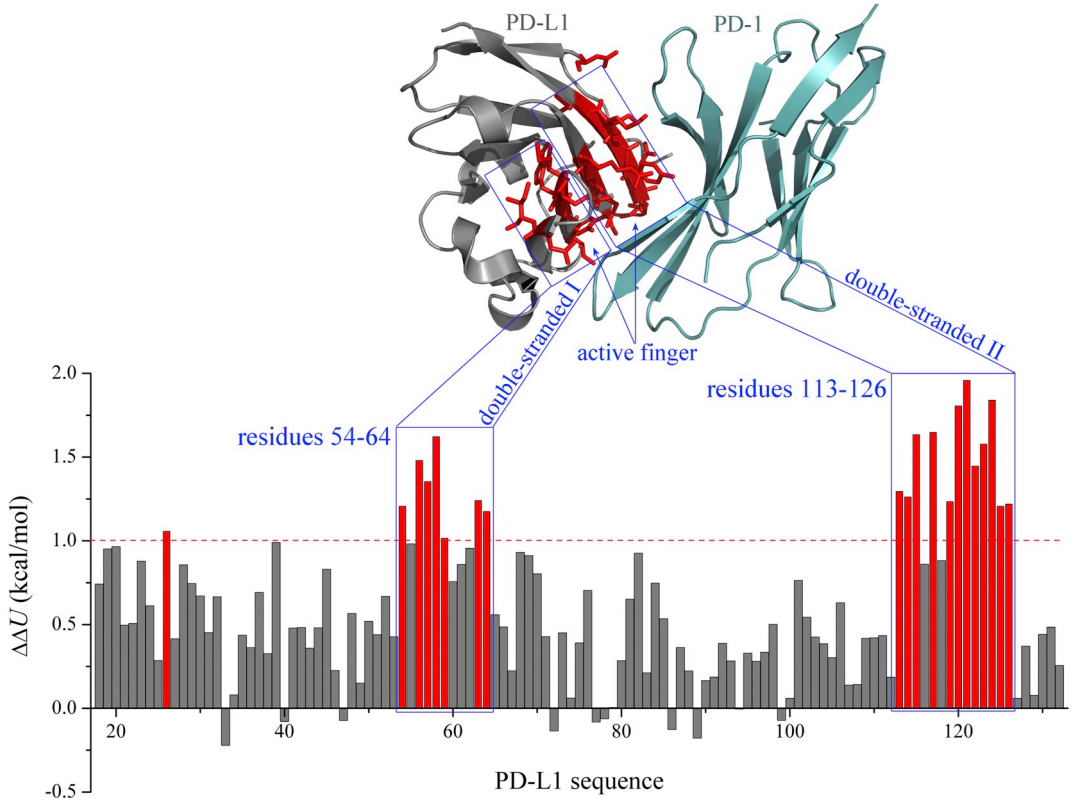

Fig. 2. Computational alanine scanning determination of the residue importance of PD-L1 (residues 18–132) binding to PD-1. The hotspot residues ($\Delta\Delta U > 1$ kcal/mol) are highlighted in red. (For interpretation of the references to colour in this figure legend, the reader is referred to the web version of this article.)

peptide (^{110}GVYRCMISYGGADYKRITVKVNA^{132}), respectively (Fig. 3A), which were then separately subjected to 250-ns MD simulations to investigate their conformational equilibrium and flexibility in free state. The root-mean-square deviation (RMSD) fluctuation profile of the two peptides during the whole simulations is shown in Fig. 3B, where their dynamics snapshots were extracted at 0, 100, 180 and 250 ns of the simulation trajectory. A strong RMSD fluctuation along the simulations can be observed, indicating that the two peptides possess large intrinsic disorder and cannot hold in the native active conformation as its location in the context of intact PD-1/PD-L1 complex interface, which would be unfavorable for the rebinding of these peptides at the interface. Conformational analysis also confirmed that both the DS-I and DS-II peptides are changed considerably from start native structure (0 ns) to final equilibrium state (250 ns), during which the large flexibility and considerable disorder are revealed. In fact, many peptides have been found to exhibit increased flexibility due to lack of protein context support [36,37], which would address unfavorable effect on the peptide binding to their native partners [38].

According to previous report, a protein–peptide binding event can be divided into two thermodynamically independent steps, namely, indirect readout and direct readout [39]. For example, as shown in Fig. 4, in the step 1 of indirect readout the DS-II peptide is intrinsically disordered in free state, which would be restricted into the native ordered conformation, thus incurring an unfavorable entropy penalty upon the binding ($-T\Delta S > 0$); in the step 2 of direct readout the native ordered conformation of DS-II peptide is bound to PD-1 amphipathic pocket to form a nonbonded interaction network across the complex interface of PD-1 with DS-II peptide, thus contributing a favorable enthalpy to the binding ($\Delta U < 0$). Therefore, the total binding free energy (ΔG) of PD-1/DS-II peptide interaction can be regarded as a compromise between the unfavorable indirect readout and favorable direct readout, *viz.* $\Delta G = \Delta U - T\Delta S$. Here, the total binding energy ΔG of DS-I and DS-II peptides to PD-1 was calculated using MM/PBSA and NMA analysis based on the complex conformational snapshots extracted from equilibrium dynamics trajectory. The ΔG can be further decomposed into direct readout ΔU and indirect readout $-T\Delta S$. The decomposed energetic terms are listed in Table 1. The ΔU values are -37.4 and -69.2 kcal/mol for DS-I and DS-II peptides, respectively,

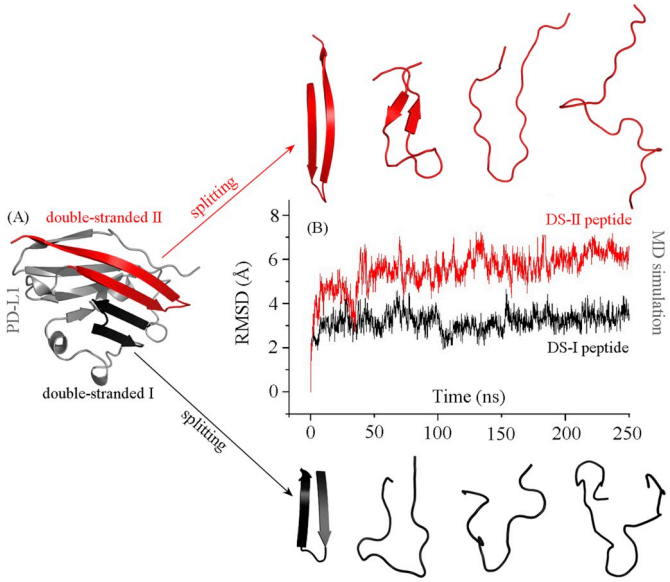

Fig. 3. (A) The double-stranded segments I and II are split from PD-L1 to derive two free peptides DS-I and DS-II; each of them is then subjected to 250-ns MD simulations for conformational relaxing and equilibrium in free state. (B) The RMSD fluctuation profile of DS-I and DS-II peptides over the simulations. The peptide conformational snapshots are shown at 0, 100, 180 and 250 ns of the simulation trajectory.

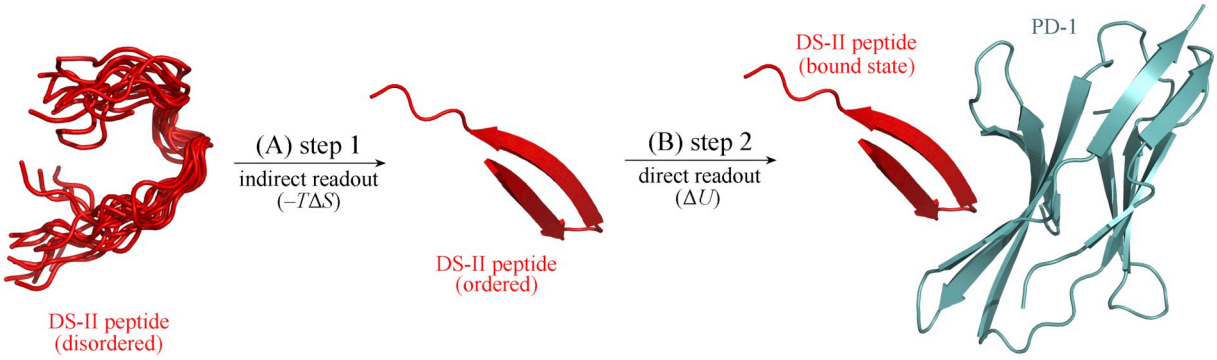

Fig. 4. Schematic representation of the direct readout and indirect readout involved in DS-II peptide binding to PD-1. (A) Step 1: the free DS-II peptide is intrinsically disordered in free state, which would be restricted into an native ordered conformation, thus incurring an unfavorable entropy penalty upon the binding ($-T\Delta S > 0$). (B) Step 2: the native ordered conformation of free DS-II peptide is bound to PD-1 amphipathic pocket to form a nonbonded interaction network across the complex interface of PD-1 with DS-II peptide, thus contributing a favorable potency to the binding ($\Delta U < 0$).

which are very favorable for the PD-1/peptide binding. However, the favorable direct readout would be largely impaired by the considerably unfavorable indirect readout ($-T\Delta S$ = 34.6 and 54.3 kcal/mol for DS-I and DS-II peptides, respectively). Consequently, the DS-I peptide cannot effectively rebind to the amphipathic pocket of PD-1 due to their large intrinsic disorder in free state ($\Delta G = -2.8$ kcal/mol), while the DS-II peptide can only bind to PD-1 with a moderate potency ($\Delta G = -14.9$ kcal/mol). Next, binding affinity of the two peptides were to PD-1 were measured by fluorescence-based assays. As might be expected, the free DS-I peptide was determined as nonbinder of DS-I (K_d = n.d.), while the free DS-II peptide only exhibited a moderate affinity towards to the protein (K_d = 109 ± 15 μM) (Table 1). Therefore, both the computational analysis and experimental assay reach an agreement that splitting of peptide segments from PD-L1 active site would influence the rebinding behavior of these peptides substantially.

3.3. Intramolecullar cyclization of double-stranded peptides

Considering that the double-stranded II segment of PD-L1 can tightly pack against the amphipathic pocket of PD-1 and its split form (*i.e.* free DS-II peptide) can also restore partial affinity towards the PD-1, we herein further investigated this segment. The segment (^{110}GVYRCMISYGGADYKRITVKVNA^{132}) covers the hotspot region (residues 113–126) that directly contact and interact with PD-1, while other

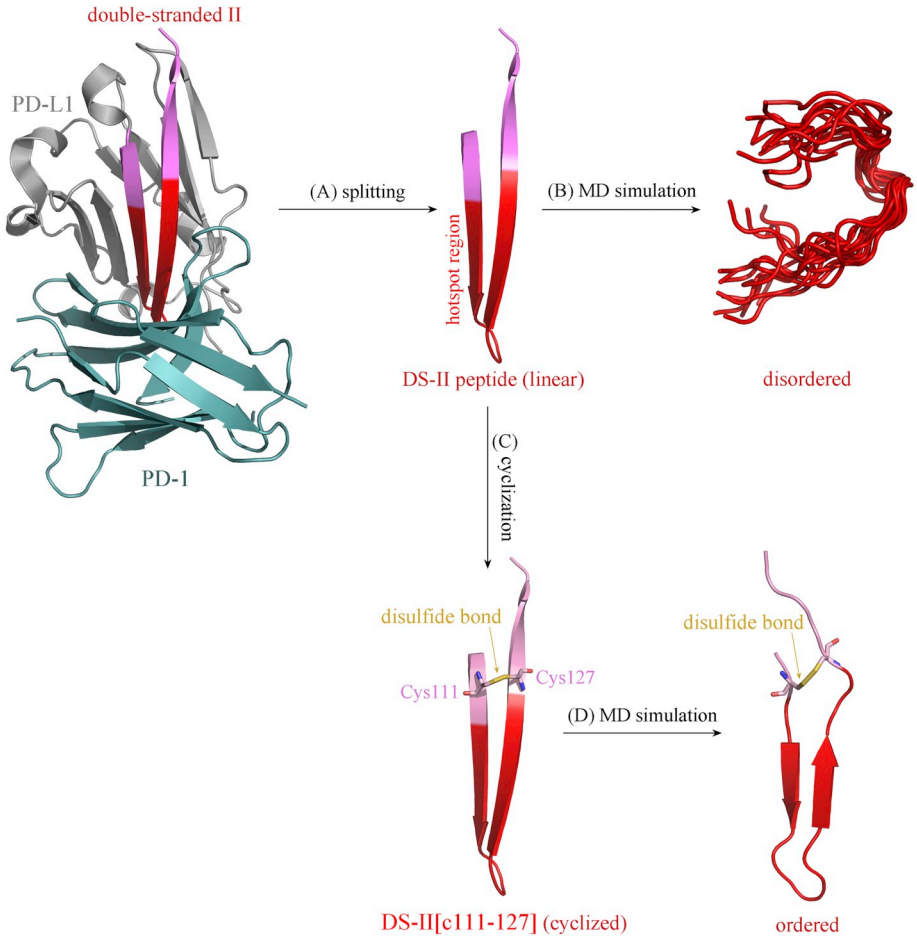

Fig. 5. (A) The double-stranded II segment is split from the complex structure of PD-L1 with PD-1 to derive a free linear DS-II peptide, where the hotspot region (residues 113–126) is highlighted in red. (B) The DS-II peptide is subjected to 250-ns MD simulations, during which the peptide exhibits a large flexibility and intrinsic disorder. (C) Two spatially vicinal residues 111 and 127 of DS-II peptide are mutated to Cys111 and Cys127, respectively, and then a disulfide bond is formed across them to generate a cyclized counterpart of linear DS-II peptide (DS-II[c111–127]). (D) The cDS-II peptide is re-subjected to 250-ns MD simulations, where an additional restraint between the two side-chain sulfur atoms of Cys111 and Cys127 is applied to mimic a disulfide bond between the two residues. During the simulations the peptide can well hold in an ordered conformation similar to its native double-stranded II structure in PD-1/PD-L1 complex interface. (For interpretation of the references to colour in this figure legend, the reader is referred to the web version of this article.)

sections can be regarded as extended N- and C-termini. Here, the segment was split from PD-1/PD-L1 complex system to derive the free DS-II peptide (Fig. 5A), which was then subjected to 250-ns MD simulations. During the simulations the peptide conformation was changed dramatically and fluctuated significantly, suggesting that the free peptide is highly flexible and possesses a large intrinsic disorder (Fig. 5B). The total binding free energy of DS-II peptide to PD-1 was calculated as $\Delta G = -14.9$ kcal/mol, which is a compromise between favorable direct readout ($\Delta U = -69.2$ kcal/mol) and unfavorable indirect readout ($-T\Delta S = 54.3$ kcal/mol), indicating a moderate interaction between the peptide and PD-1.

According to above discussion, the linear DS-II peptides derived from the active finger of PD-L1 protein is intrinsically disordered, thus unfavorable to their interaction with PD-1 due to large entropy penalty. Instead of traditionally increasing intermolecular interaction enthalpy, we herein attempted to improve PD-1/DS-II binding affinity by minimizing entropy cost of the binding [40,41]. Cyclization strategy has recently been successfully utilized to constrain peptide conformation for therapeutic purpose [25,26]. By visually examining the native conformation of double-stranded II segment in the interfacial context of PD-1/PD-L1 complex it is evident that the segment consists of two antiparallel β-strands and exhibits a U-shaped form that is suited for cyclization. A further examination of the native segment found that the residue pairs Val111-Thr127 and Gly110-Val128 are (i) spatially vicinal to each other, (ii) across the two β-strand arms, and (iii) out of the core hotspot region. Therefore, we considered to add a disulfide bridge across them to define intramolecular cyclic peptides. As shown in Fig. 5C, for example, the DS-II peptide residues Val111 and Thr127 were mutated to Cys111 and Cys127, respectively, and the linear peptide was then cyclized by adding a disulfide bond across the two spatially vicinal residues, consequently resulting in a cyclic peptide DS-II[c111–127], which was re-subjected to 250-ns MD simulations, where an additional restraint between the two side-chain sulfur atoms of Cys111 and Cys127 was applied to mimic a disulfide bond between the two residues. During the simulations the peptide can well hold in an ordered conformation similar to its native double-stranded II configuration in PD-1/PD-L1 complex interface (Fig. 5D).

In order to substantiate the computational simulations, circular dichroism (CD) spectroscopy was used to characterize the solution secondary structure of linear DS-II peptide and cyclic DS-II[c111–127] peptide in free state. As shown in Fig. 6A, the DS-II peptide has a spectral profile of disordered conformation with low structured rate, characterized by a single negative band below 210 nm. In contrast, the spectral profile is changed considerably upon Cys111-Cys127 cyclization (to create DS-II[c111–127] peptide), which has a strong stranded propensity with a positive band at ~195 nm and a negative band at ~217 nm. This meets the typical β-sheet feature [42]. As listed in Table 1, the cyclization can considerably improve total binding energy ΔG from −14.9 kcal/mol (linear DS-II peptide) to −27.5 kcal/mol (cyclic DS-II[c111–127] peptide). As might be expected, energetic decomposition revealed a significant reduction in unfavorable indirect readout ($-T\Delta S$ decreases from 54.3 to 38.7 kcal/mol) and also a moderate reduction in favorable direct readout (ΔU changes from −69.2 to −66.2 kcal/mol) upon the cyclization. This is not unexpected if considering that cyclization may slightly alter peptide native conformation in PD-L1 active site, thus impairing some established nonbonded interactions and reducing packing tightness at the formed complex interface [43]. The binding affinity of cyclic DS-II[c111–127] peptide was determined as $K_d = 28.0 \pm 4.2$ μM, which was improved by ~4-fold relative to linear DS-II peptide ($K_d = 109 \pm 15$ μM) (Fig. 6B), confirming that the cyclization can indeed improve the binding capability of PD-L1 derived peptide to PD-1 substantially.

Considering that the one N-terminal residue G^{110} and the five C-terminal residues ^{128}VKVNA^{132} of DS-II[c111–127] peptide do not belong to hotspot region of the peptide and are out of the peptide intramolecular cycle — they should not contribute effectively to the PD-1/DS-II[c111–127] interaction, we just removed them from two termini of the peptide to obtain a truncated version of cyclic peptide ΔDS-II [c111–127]. Energetic calculations suggested that the truncation can further enhance the peptide binding energy to −31.3 kcal/mol, which was confirmed by affinity assay with K_d change to 17.5 ± 3.1 μM for the truncated peptide (Fig. 6B). The affinity improvement is also primarily contributed by the decrease in indirect readout due to removal of the peptide free termini, albeit the improvement is not significant. Similarly, the cyclic peptide ΔDS-II[c110–128] can also be obtained *via* mutation, cyclized and truncated from linear DS-II peptide, and its binding capability to PD-1 was analysis using energetic calculations and affinity assays. As shown in Table 1 and Fig. 6B, the ΔDS-II[c110–128] can bind similarly with ΔDS-II[c111–127] ($\Delta G = -30.1$ *versus* −31.3 kcal/mol and $K_d = 11.6 \pm 2.3$ *versus* 17.5 ± 3.1 μM), suggesting that different terminal cyclizations of the linear DS-II peptide do not influence the peptide binding behavior substantially. The minimization of unfavorable indirect readout, but not the maximization of favorable direct readout, is the primary factor of cyclization

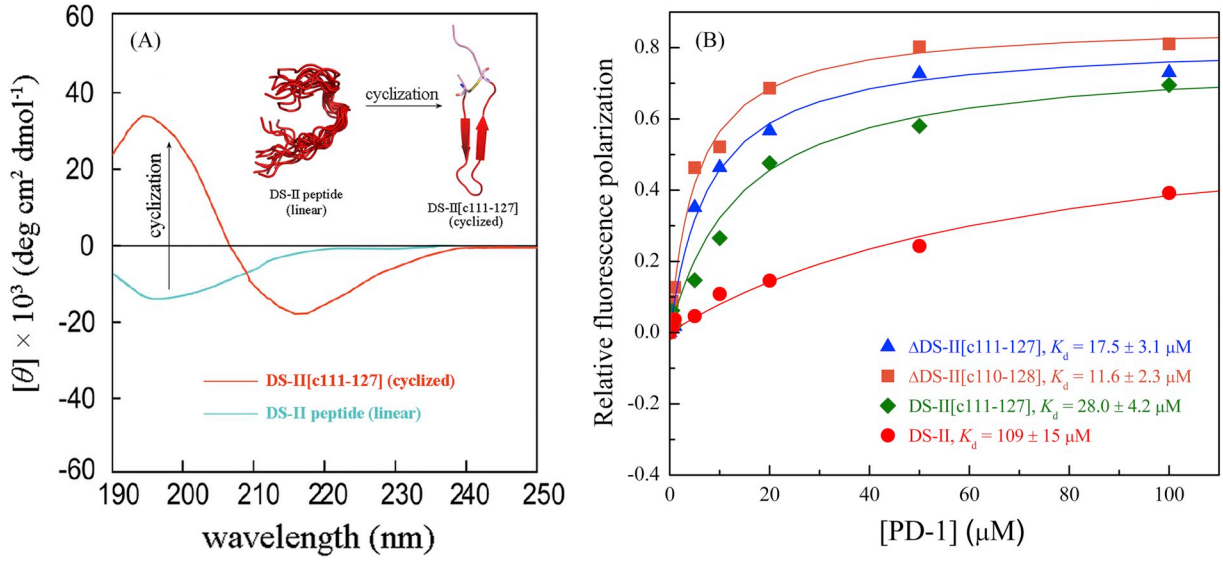

Fig. 6. (A) CD spectra of linear DS-II peptide and cyclized DS-II[c111–127] peptide in wavelength range 190–250 nm. (B) Binding curves of linear DS-II peptide as well as its three cyclized counterparts DS-II[c111–127], ΔDS-II[c111–127] and ΔDS-II[c110–128] to the recombinant protein of PD-1.

contributing to PD-1/peptide affinity improvement.

4. Conclusions

Two linear peptide segments DS-I and DS-II were stripped from PD-1/PD-L1 complex structure; they represent the double-stranded I and II of PD-L1 active finger and are expected as self-inhibitory peptides to rebind at the complex interface to disrupt the complex interaction. The DS-II peptide was found to have a moderate affinity to PD-1, which was then truncated and cyclized to optimize its structure and to reduce its flexibility, resulting in three modified cyclic peptides DS-II[c111–127], ΔDS-II[c111–127] and ΔDS-II[c110–128]. Fluorescence-based assays confirmed that the modification can considerably improve peptide affinity by minimizing entropy penalty upon binding, with affinity increase by, at most, ~10-fold. It is worth noting that the current work has been done at molecular level and tested only for the peptide binding potency to PD-1, but their inhibitory capability on PD-1/PD-L1 interaction as well as therapeutic activity against breast cancer were not examined here. In next works, we plan to further perform *in vitro* and *in vivo* studies for these rationally designed peptides to investigate their biological function at cellular and animal levels.

Acknowledgements

This work was supported by the HHAFU Foundation.

Conflict of interest

All the authors declare that there are no conflicts of interest.

References

[1] J.A. Marin-Acevedo, B. Dholaria, A.E. Soyano, K.L. Knutson, S. Chumsri, Y. Lou, Next generation of immune checkpoint therapy in cancer: new developments and challenges, J. Hematol. Oncol. 11 (2018) 39.
[2] D.M. Pardoll, The blockade of immune checkpoints in cancer immunotherapy, Nat. Rev. Cancer 12 (2012) 252–264.
[3] K. Magiera-Mularz, L. Skalniak, K.M. Zak, B. Musielak, E. Rudzinska-Szostak, L. Berlicki, J. Kocik, P. Grudnik, D. Sala, T. Zarganes-Tzitzikas, S. Shaabani, A. Dömling, G. Dubin, T.A. Holak, Bioactive macrocyclic inhibitors of the PD-1/PD-L1 immune checkpoint, Angew. Chem. Int. Ed. Engl. 56 (2017) 13732–13735.
[4] K.M. Zak, P. Grudnik, K. Magiera, A. Dömling, G. Dubin, T.A. Holak, Structural biology of the immune checkpoint receptor PD-1 and its ligands PD-L1/PD-L2, Structure 25 (2017) 1163–1174.
[5] M. Konstantinidou, T. Zarganes-Tzitzikas, K. Magiera-Mularz, T.A. Holak, A. Dömling, Immune checkpoint PD-1/PD-L1: is there life beyond antibodies? Angew. Chem. Int. Ed. Engl. 57 (2018) 4840–4848.
[6] A. Swoboda, R. Nanda, Immune checkpoint blockade for breast cancer, Cancer Treat. Res. 173 (2018) 155–165.
[7] K.M. Hargadon, C.E. Johnson, C.J. Williams, Immune checkpoint blockade therapy for cancer: an overview of FDA-approved immune checkpoint inhibitors, Int. Immunopharmacol. 62 (2018) 29–39.
[8] S.C. Wei, C.R. Duffy, J.P. Allison, Fundamental mechanisms of immune checkpoint blockade therapy, Cancer Discov. 8 (2018) 1069–1086.
[9] K.M. Zak, R. Kitel, S. Przetocka, P. Golik, K. Guzik, B. Musielak, A. Dömling, G. Dubin, T.A. Holak, Structure of the complex of human programmed death 1, PD-1, and its ligand PD-L1, Structure 23 (2015) 2341–2348.
[10] J. Lu, K. Zhou, X. Yin, H. Xu, B. Ma, Molecular insight into the T798M gatekeeper mutation-caused acquired resistance to tyrosine kinase inhibitors in ErbB2-positive breast cancer, Comput. Biol. Chem. 78 (2019) 290–296.
[11] N. London, B. Raveh, D. Movshovitz-Attias, O. Schueler-Furman, Can self-inhibitory peptides be derived from the interfaces of globular protein-protein interactions? Proteins 78 (2010) 3140–3149.
[12] C. Yang, S. Zhang, P. He, C. Wang, J. Huang, P. Zhou, Self-binding peptides: folding or binding? J. Chem. Inf. Model. 55 (2015) 329–342.
[13] C. Yang, S. Zhang, Z. Bai, S. Hou, D. Wu, J. Huang, P. Zhou, A two-step binding mechanism for the self-binding peptide recognition of target domains, Mol. BioSyst. 12 (2016) 1201–1213.
[14] Z. Bai, S. Hou, S. Zhang, Z. Li, P. Zhou, Targeting self-binding peptides as a novel strategy to regulate protein activity and function: a case study on the proto-oncogene tyrosine protein kinase c-Src, J. Chem. Inf. Model. 57 (2017) 835–845.
[15] H.M. Berman, J. Westbrook, Z. Feng, G. Gilliland, T.N. Bhat, H. Weissig, I.N. Shindyalov, P.E. Bourne, The protein data bank, Nucleic Acids Res. 28 (2000) 235–242.
[16] Y. Duan, C. Wu, S. Chowdhury, M.C. Lee, G. Xiong, W. Zhang, R. Yang, P. Cieplak, R. Luo, T. Lee, J. Caldwell, J. Wang, P. Kollman, A point-charge force field for molecular mechanics simulations of proteins based on condensed-phase quantum mechanical calculations, J. Comput. Chem. 24 (2003) 1999–2012.
[17] W.L. Jorgensen, J. Chandrasekhar, J.D. Madura, R.W. Impey, M.L. Klein, Comparison of simple potential functions for simulating liquid water, J. Phys. Chem. 79 (1983) 926–935.
[18] C. Yang, C. Wang, S. Zhang, J. Huang, P. Zhou, Structural and energetic insights into the intermolecular interaction among human leukocyte antigens, clinical hypersensitive drugs and antigenic peptides, Mol. Simul. 41 (2015) 741–751.
[19] P. Zhou, S. Zhang, Y. Wang, C. Yang, J. Huang, Structural modeling of HLA-B1502 peptide carbamazepine T-cell receptor complex architecture: implication for the molecular mechanism of carbamazepine-induced Stevens-Johnson syndrome toxic epidermal necrolysis, J. Biomol. Struct. Dyn. 34 (2016) 1806–1817.
[20] L. Saíz-Urra, M.A. Cabrera, M. Froeyen, Exploring the conformational changes of the ATP binding site of gyrase B from Escherichia coli complexed with different established inhibitors by using molecular dynamics simulation: protein-ligand interactions in the light of the alanine scanning and free energy decomposition methods, J. Mol. Graph. Model. 29 (2011) 726–739.
[21] Z. Li, F. Yan, Q. Miao, Y. Meng, L. Wen, Q. Jiang, P. Zhou, Self-binding peptides: binding-upon-folding versus folding-upon-binding, J. Theor. Biol. 469 (2019) 25–34.
[22] J.P. Ryckaert, G. Ciccotti, H.J.C. Berendsen, Numerical integration of the Cartesian equations of motion of a system with constraints: molecular dynamics of n-alkanes, J. Comput. Phys. 23 (1997) 327–341.
[23] T. Darden, D. York, L. Pedersen, Particale mesh Ewald and N.log(N) method for Ewald sums in large systems, J. Chem. Phys. 98 (1983) 10089–10092.
[24] N. Homeyer, H. Gohlke, Free energy calculations by the molecular mechanics Poisson-Boltzmann surface area method, Mol. Inf. 31 (2012) 114–122.
[25] W. Zhang, B. Zhong, C. Zhang, Y. Wang, S. Guo, C. Luo, Y. Zhan, Structural modeling of osteoarthritis ADAMTS4 complex with its cognate inhibitory protein TIMP3 and rational derivation of cyclic peptide inhibitors from the complex interface to target ADAMTS4, Bioorg. Chem. 76 (2018) 13–22.
[26] T. Wu, P. He, W. Wu, Y. Chen, F. Lv, Targeting oncogenic transcriptional corepressor Nac1 POZ domain with conformationally constrained peptides by cyclization and stapling, Bioorg. Chem. 80 (2018) 1–10.
[27] Y. Zhang, K. Schulten, M. Gruebele, P.S. Bansal, D. Wilson, N.L. Daly, Disulfide bridges: bringing together frustrated structure in a bioactive peptide, Biophys. J. 110 (2016) 1744–1752.
[28] J. Wang, J. Zhang, X. Sun, C. Liu, X. Li, L. Chen, Molecular design of sequence-minimized, structure-optimized, and hydrocarbon-stapled helix-helix interactions in the trimer-of-hairpins motif of pediatric pneumonia RSV-F protein, Chem. Biol. Drug Des. (2019), https://doi.org/10.1111/cbdd.13501.
[29] N.J. Moerke, Fluorescence polarization (FP) assays for monitoring peptide-protein or nucleic acid-protein binding, Curr. Protoc. Chem. Biol. 1 (2009) 1–15.
[30] T. Wu, P. He, W. Wu, Y. Chen, F. Lv, Targeting oncogenic transcriptional corepressor Nac1 POZ domain with conformationally constrained peptides by cyclization and stapling, Bioorg. Chem. 80 (2018) 1–10.
[31] K. Chen, L. Huang, B. Shen, Rational cyclization-based minimization of entropy penalty upon the binding of Nrf2-derived linear peptides to Keap1: a new strategy to improve therapeutic peptide activity against sepsis, Biophys. Chem. 244 (2019) 22–28.
[32] T. Kortemme, D.E. Kim, D. Baker, Computational alanine scanning of protein-protein interfaces, Sci. STKE 2004 (2004) (pl2).
[33] F. Tian, Y. Lv, P. Zhou, L. Yang, Characterization of PDZ domain-peptide interactions using an integrated protocol of QM/MM, PB/SA, and CFEA analyses, J. Comput. Aided Mol. Des. 25 (2011) 947–958.
[34] F. Tian, R. Tan, T. Guo, P. Zhou, L. Yang, Fast and reliable prediction of domain–peptide binding affinity using coarse-grained structure models, Biosystems 113 (2013) 40–49.
[35] Z. Li, Q. Miao, F. Yan, Y. Meng, P. Zhou, Machine learning in quantitative protein-peptide affinity prediction: implications for therapeutic peptide design, Curr. Drug Metab. 20 (2019) 170–176.
[36] P. Zhou, S. Hou, Z. Bai, Z. Li, H. Wang, Z. Chen, Y. Meng, Disrupting the intramolecular interaction between proto-oncogene c-Src SH3 domain and its self-binding peptide PPII with rationally designed peptide ligands, Artif. Cells Nanomed. Biotechnol. 46 (2018) 1122–1131.
[37] P. Zhou, Q. Miao, F. Yan, Z. Li, Q. Jiang, L. Wen, Y. Meng, Is protein context responsible for peptide-mediated interactions? Mol. Omics (2019), https://doi.org/10.1039/c9mo00041k.
[38] H. Yu, P. Zhou, M. Deng, Z. Shang, Indirect readout in protein–peptide recognition: a different story from classical biomolecular recognition, J. Chem. Inf. Model. 54 (2014) 2022–2032.
[39] H. Hu, S. Yang, J. Zheng, G. Mao, Structure-based derivation of peptide inhibitors to target TGF-β1 receptor for the suppression of hypertrophic scarring fibroblast activation, Chem. Biol. Drug Des. 90 (2017) 345–351.
[40] P. Zhou, C. Yang, Y. Ren, C. Wang, F. Tian, What are the ideal properties for functional food peptides with antihypertensive effect? A computational peptidology approach, Food Chem. 141 (2013) 2967–2973.
[41] P. Zhou, C. Wang, F. Tian, Y. Ren, C. Yang, J. Huang, Biomacromolecular quantitative structure-activity relationship (BioQSAR): a proof-of-concept study on the modeling, prediction and interpretation of protein–protein binding affinity, J. Comput. Aided Mol. Des. 27 (2013) 67–78.
[42] N.J. Greenfield, Using circular dichroism spectra to estimate protein secondary structure, Nat. Protoc. 1 (2006) 2876–2890.
[43] H. Luo, T. Du, P. Zhou, L. Yang, H. Mei, H. Ng, W. Zhang, M. Shu, W. Tong, L. Shi, D.L. Mendrick, H. Hong, Molecular docking to identify associations between drugs and class I human leukocyte antigens for predicting idiosyncratic drug reactions, Comb. Chem. High Throughput Screen. 18 (2015) 296–304.